Acta Cryst A FOUNDATIONS ADVANCES

ISSN 2053-2733

Crystallographic descriptions of regular 2-periodic weavings of threads, loops and nets

Michael O'Keeffe[a] and Michael M. J. Treacy[b]*

[a]School of Molecular Sciences, Arizona State University, 551 E. University Drive, Tempe, Arizona 85281, USA, and [b]Department of Physics, Arizona State University, 550 E. Tyler Mall, Tempe, Arizona 85287, USA. *Correspondence e-mail: treacy@asu.edu

Received 4 October 2019
Accepted 29 January 2020

Edited by U. Grimm, The Open University, UK

Keywords: 2-periodic weavings; nets; threads; loops; regular structures.

Supporting information: this article has supporting information at journals.iucr.org/a

Piecewise linear descriptions are presented of weavings of threads, loops and 2-periodic nets. Crystallographic data are provided for regular structures, defined as those with one kind (symmetry-related) of vertex (corner) and edge (stick). These include infinite families of biaxial thread weaves, interwoven square lattices (**sql**), honeycomb (**hcb**) nets, and tetragonal and hexagonal polycatenanes.

1. Introduction

Weaving of threads into fabrics is one of the oldest of human creative activities. More recently it has become of interest in the design, synthesis and description of an emerging class of network crystalline materials in which the vertices and edges of the net are molecular units. In a recent paper (Liu *et al.*, 2018), which reviewed material structures based on weaving of molecular 'threads', it was argued from a chemical perspective that it was most appropriate to consider such structures as piecewise linear, *i.e.* they are composed of linear segments ('sticks') that meet at divalent vertices ('corners'). With reference to the most symmetrical embedding of a structure, a *transitivity p q r* is defined to indicate that there are *p* kinds (related by symmetry) of corner, *q* kinds of stick and *r* kinds of thread. In this paper we are concerned only with *regular* structures – those with transitivity 1 1 1. In the jargon, corner- (or vertex-)transitive structures are *isogonal*, stick- (or edge-)transitive structures are *isotoxal* and thread-transitive structures are *isonemal*.

In this work, our goal is to identify those periodic structures that are most suitable for designed synthesis by assembly from molecular components [reticular chemistry (Yaghi *et al.*, 2003)]. At the molecular level, structures are almost universally made of such components joined by straight links. It is a basic tenet of reticular chemistry that the most favourable structures to target are those with minimal transitivity (Li *et al.*, 2014). 'Crystallographic description' of the title refers to structure description in terms of symmetry, unit-cell parameters and coordinates of vertices. To complete the description, links (edges) are explicitly specified ('from' vertices and 'to' vertices). We believe that the combination of the piecewise linear construction, with the crystallographic description, is novel. For other approaches to weaving we refer readers to Thompson & Hyde (2018, and references therein).

Obtaining the maximum-symmetry embedding of a weave, along with its minimal transitivity representation, are

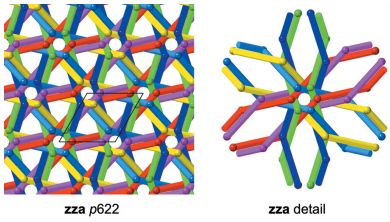

surprisingly difficult problems. Weavings are really in the same category as knots, and determining the symmetry of knots is not straightforward (*e.g.* Flapan, 1988) in contrast to the situation with periodic graphs (Treacy *et al.*, 1997; Delgado-Friedrichs & O'Keeffe, 2003). Indeed, we report below on structures that we described earlier as having transitivity 1 2 1 but which actually have a higher-symmetry description with transitivity 1 1 1. These earlier descriptions were not wrong, but just not optimal. Here, we restrict ourselves to structures with transitivity 1 1 1, and so they must be optimal. We call them *regular* by analogy with polyhedra and 2-periodic tilings, for which the term *regular* is universally applied to structures with transitivity (vertices edges faces) 1 1 1.

Here, we extend the earlier discussion to include additional regular 2-periodic thread weaves and polycatenanes and also include interwoven 2-periodic nets.

Over the years the topic of weaving has accumulated a huge variety of special terms. Here, we examine 2-periodic interwoven structures that have the symmetry of a layer group. Curiously, most mathematical papers discussing weaving omit the symmetry aspect, but we note a significant exception (Roth, 1993). The 2-periodic lattice defines what we term the *lattice plane* [this is the 'master net' of Thompson & Hyde (2018)]. In a weaving of conventional *fabrics*, if the threads are pulled straight they intersect in the lattice plane and the points of intersection fall on the vertices of a 2-periodic net. In a *biaxial* (2-way) weave the net is that of the square lattice, **sql**. In a *triaxial* (3-way) weave the net is either that of the kagome pattern, **kgm**, or the hexagonal lattice **hxl**. Here, bold, lower-case, three-letter symbols are RCSR (Reticular Chemistry Structure Resource) symbols (O'Keeffe *et al.*, 2008). In some other patterns of interlaced threads, if the threads are pulled straight (and allowed to pass through each other) they fall into parallel rows. We refer to this as *chain-link* weaving as this is the pattern used in chain-link fences. The term also applies to the patterns of conventional knitting.

We define a quantity, *girth*, as the ratio of the shortest distance between sticks and the stick length (all the reported structures have just one kind of stick, which we treat as freely hinged cylindrical rods). In finding an optimal embedding we search for the parameters that give the largest girth. This maximum girth is the ratio of the stick diameter to the length of the thickest stick compatible with that weave. The purist may note that 'girth' normally refers to circumference rather than diameter. They can multiply our reported values by π.

The concept of girth was introduced in our earlier paper (Liu *et al.*, 2018) and is inspired by earlier work on curved threads for knots (Stasiak *et al.*, 1998) and weavings (Evans *et al.*, 2015). As we show below, plots of girth as a function of structural parameters (unit cell and coordinates) allow the identification and mapping of regions of existence of topologically distinct structures. It is of practical interest that larger-girth structures will likely be more amenable to designed synthesis. We note that non-edge-transitive structures (*i.e.* those involving more than one kind of stick, $q > 1$) will entail multiple girths.

2. Methods

Weaves are found in those 67 (out of the 80) layer groups that do not have an in-plane mirror. Regular weaves are found by placing a single vertex at x, y, z and examining systematically edges to the symmetry-related vertices. For this study, this procedure was done by hand and the list of weaves presented here is unlikely to be complete. For example, we have not yet examined systematically the rectangular or oblique weaves.

Maximum-girth embeddings were found using the 3-periodic space group obtained from the layer group by changing the symbol p or c to P or C, then building an $11\mathbf{a} \times 11\,\mathbf{b} \times 3\mathbf{c}$ domain of unit cells, where the edge vectors **a** and **b** lie in the plane of the weave. The third cell edge vector, **c**, points out of the plane. The 'fundamental stick' is nominally associated with the central cell, although x, y, z can attain values outside the range 0 to 1, whereupon the fundamental stick may not even intersect the central cell. Some weaves connect across multiple cells, and larger domain sizes in the **a**, **b** plane were sometimes needed for parts of this study. Depending on the crystal symmetry, and the local symmetry of the vertex x, y, z, up to five parameters were varied (x, y, z, and the ratios b/a and c/a, with a held at $a = |\mathbf{a}| = 1$) in order to identify the largest nearest-neighbour girth – that is, the closest stick distance divided by the stick length. Sticks directly linked to the fundamental stick were excluded from the list of neighbouring sticks for girth calculations since the closest distance between linked sticks is always zero. In this study, we examined those groups with fixed inter-axial angles, viz. hexagonal, trigonal, tetragonal and rectangular groups. In regular weaves, all sticks (edges) are symmetry related and have identical lengths and girths. The downhill simplex method of Nelder & Mead (1965) was used to find the maximum-girth values. This was done by posing the problem as a convex one – the minimization of the value of 1/girth – using the implementation provided in *Numerical Recipes in C* by Press *et al.* (1992).

To compute the girth, sticks were treated as line segments, with a length and direction, between a 'from' vertex and a 'to' vertex. There are three scenarios to consider when evaluating the proximity of two line segments (infinitesimally thin sticks). These are when the point of closest approach: (i) lies on each stick, away from their ends; (ii) is between the end of one stick, but lying on the second stick; (iii) is between the ends of both sticks. The closest distance between two line segments, or between a line segment and a point, or between two points is found by simple geometry. That closest distance determines the maximum allowed diameter of the stick (cylinder) where cylinders just touch. Strictly speaking, if connected sticks are treated uncompromisingly as rigid cylinders, then only straight 'threads' are possible, since any flexing at the joints between cylinders (vertices) will automatically result in an overlap at the ends. We relaxed the no-overlap condition at the vertices, allowing cylinders to hinge with no penalty. As a result, our sticks therefore have bevelled ends and the maximum girth allowed is 1. This is a reasonable relaxation of the geometrical

Table 1
Crystallographic data for regular univariant (*zc*/*a*) weaves.

For drawing in 3-periodic groups convert the lattice symbol to upper case (*p* to *P*) and make *c*/*a* sufficiently large that layers do not overlap. Entries are in the order they appear in the text.

Symbol	Group	From	To	*zc*/*a*	Girth	Angle (°)
sql-w	*p*4/*nbm*	3/4, 1/4, *z*	1/4, 3/4, −*z*	0.2973	0.4142	99.88
sql-w12	*p*4/*n*	3/4, 1/4, *z*	5/4, 7/4, −*z*	0.6648	0.0828	99.88
sql-w23	*p*4/*n*	3/4, 1/4, *z*	5/4, 11/4, −*z*	1.0719	0.0319	99.88
sql-w14	*p*4/*n*	3/4, 1/4, *z*	9/4, 11/4, −*z*	1.2258	0.0244	99.88
kgm-w	*p*622	1/2, 0, *z*	1/2, 1/2, −*z*	0.1768	0.3333	109.47
wvm	*p*622	1/2, 0, *z*	3/2, 1/2, −*z*	0.4030	0.1547	94.12
sql-c5	*p*4/*n*	1/4, 1/4, *z*	7/4, 3/4, −*z*	0.5590	0.1633	70.53
sql-c13	*p*4/*n*	1/4, 1/4, *z*	11/4, 3/4, −*z*	0.9014	0.0628	70.53
sql-c17	*p*4/*n*	1/4, 1/4, *z*	11/4, 7/4, −*z*	1.0308	0.0480	70.53
hcb-c3	*p*$\bar{3}$1*m*	0, 0, *z*	1, 0, −*z*	0.3535	0.3333	90.00
hcb-c6	*p*622	1/3, 2/3, *z*	1/3, −1/3, −*z*	0.4653	0.1547	78.69
hcb-c21	*p*$\bar{3}$	0, 0, *z*	1, 3, −*z*	0.9354	0.4762	90.00
hcb-c7	*p*$\bar{3}$	1/3, 2/3, *z*	2/3, 7/3, −*z*	0.5401	0.1429	90.00
hcb-c13	*p*$\bar{3}$	1/3, 2/3, *z*	8/3, 4/3, −*z*	0.7360	0.0769	90.00
hcb-c19	*p*$\bar{3}$	1/3, 2/3, *z*	2/3, 10/3, −*z*	0.8897	0.0526	90.00

constraint because most girths in weaves are much less than 1. Further, discs (where girth > 1), hinged across their diameters, make inherently unsuitable 'sticks' for generating weaves.

3. Biaxial weaves

There is extensive literature and specialized nomenclature on biaxial weaves. Normally *fabrics* are made on a *loom* with one set of threads, the *warp*, in place and the orthogonal threads, the *weft* (or '*woof*'), interwoven. The pattern of weaving, when viewed from one side, can be expressed as a grid of squares coloured black for weft on top (*i.e.* visible), or white for warp on top, as shown later. Such patterns are known as *designs*. The classic source of designs is *Watson's Advanced Textile Design* (Grosicki, 1977). Systematic compilations of isonemal designs (some hundreds) are in the work of Grünbaum & Shephard (1980, 1985, 1986, 1988).

3.1. Regular weavings based on the square lattice net sql

The simplest biaxial weave is *plain weave*, also called *calico*, *box* and *tabby weave*. In this weave, threads cross in the simple repeating pattern under, over, ... The symmetry is *p*4/*nbm*

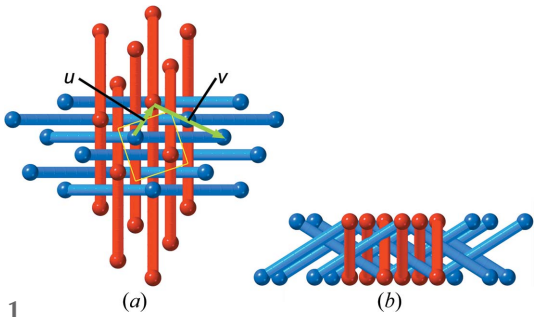

Figure 1
Generation of the weave **sql-w12**. (*a*) shows that the link between corners is a 'knight's move' *u*, *v* on a square lattice. (*b*) The side view illustrating the three-dimensional nature of the weave.

(Roth, 1993) and was identified as the regular biaxial weave (Liu *et al.*, 2018). Here, we identify an infinite family of regular weaves with symmetry *p*4/*n*. This is derived as follows. We start with two parallel square lattices (with orthogonal lattice vectors **a** and **b**) of points, one above and the other below the lattice plane of the weave. We next connect a point on one of the lattices to a symmetry-related point on the other lattice, separated laterally by the in-plane vector *u***a** + *v***b**, *u* and *v* being integers. This constitutes a stitch through the plane of the weave. If this is embedded in a doubled cell, with an appropriate origin, then a 4/*n* axis will generate a weave (alternating 'up' and 'down' stitches) for certain values of *u* and *v*, as illustrated in Fig. 1. With *u* = 0 and *v* = 1 the plain weave results. It is straightforward to see that the permissible values of *u* and *v* for distinct weaves are just those of the generalized knight's move on an infinite square chess board (Delgado-Friedrichs & O'Keeffe, 2009). Specifically, the constraints are: (*a*) *u* < *v*; (*b*) *u*, *v* are co-prime (*i.e.* no common factor); (*c*) *u*, *v* are of opposite parity (one odd, one even).

Fig. 2 illustrates some of these weaves. The threads are here depicted by black and white to mimic the design of the weave.

The number of crossings in the unit cell is 2*t* where $t = (u^2 + v^2)$. The possible values of *t* are therefore 'Pythagorean' numbers, the sum of two integers squared. Possible values of *t* are 5, 13, 17, 25, 29, 37, ... It is also the case that there are 2*t* crossings in the up–down repeat of the thread. The plain weave has the RCSR symbol **sql-w**. We identify the others as **sql-w12**, **sql-w23** *etc.* where the numbers are *uv*. Weaves with *v* = *u* + 1 are known as sponge weaves. We have not seen the others explicitly described. Data for maximum-girth embeddings, or representative examples, are given in Table 1. Notable is that the angle at the corner is always ∼99.9°

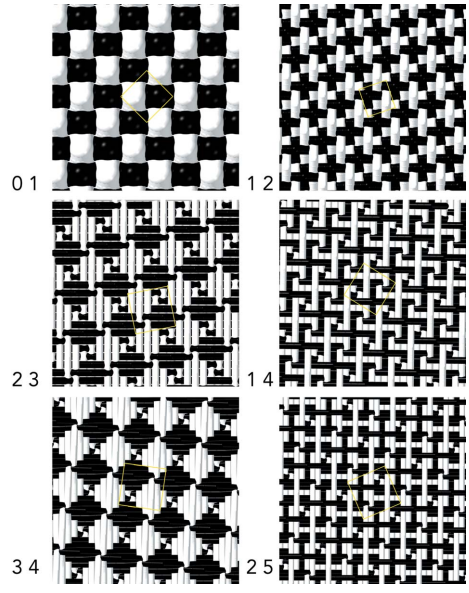

Figure 2
Some regular weaves, **sql-w*uv***, drawn with black and white for the warp (horizontal threads) and weft (vertical threads), respectively. The numbers are the values of *u* and *v*. 1 2, 2 3 and 3 4 are examples of *sponge weaves*.

Table 2
Crystallographic data for bi- and trivariant regular weavings and polycatenanes.

Vertices at x, y, z except for **wvc** $(x, -x, z)$, **cmt** in $p\bar{3}1m$ $(x, 0, z)$ and **sql-c**** $(0, y, z)$. Data can be plotted for any values of the cell parameters a, $b = a$ and c, with z calculated from zc/a using the 3-periodic group derived from the given group by capitalizing the lattice symbol (p). Where applicable, data are for second-origin setting of groups. Entries are in the order they appear in the text.

Symbol	Group	Edge to	x	y	zc/a	Girth	Angle (°)
pcu-w-c (wvc)	$p4/nbm$	$1/2+x, 1/2-x, -z$	0.1667	−0.1667	0.2500	0.2722	109.47
pcu-w12-c	$p4/n$	$x+3/2, y-1/2, -z$	0.3283	0.1128	0.5590	0.0544	109.47
pcu-w23-c	$p4/n$	$x+5/2, y-1/2, -z$	0.3258	0.1016	0.9014	0.0209	109.47
sql-w12-c	$p4/n$	$x+3/2, y-1/2, -z$	0.0536	0.0932	0.5590	0.0544	109.47
sql-w23-c	$p4/n$	$x+5/2, y-1/2, -z$	0.1014	0.1464	0.9014	0.0209	109.47
sql-ww	$p422$	$1+y, x, -z$	0.2675	0.0304	0.333	0.1884	85.60
sql-ww*	$p\bar{4}b2$	$1/2+y, 1/2+x, -z$	−0.0269	0.2335	0.3069	0.1904	89.29
sql-ww**	$p42_12$	$1+y, x, -z$	0.2050	0.1336	0.3500	0.1378	74.74
kgm-ww	$p622$	$1+y, x, -z$	0.3551	−0.0318	0.2237	0.1687	91.34
hcb-w	$p321$	$y, 1+x, -z$	0.4047	0.4272	0.3981	0.0796	47.07
hcb-w-c	$p622$	$y, 1+x, -z$	0.3697	0.4608	0.2918	0.0688	57.17
zza	$p622$	$y-x, 1+y, -z$	−0.0055	0.2308	0.3441	0.1006	99.35
zzb	$p422$	$1-y, 2-x, -z$	0.0866	0.2335	0.8171	0.0420	33.69
zzc	$p42_12$	$2-y, 1-x, -z$	0.2441	0.0488	0.6533	0.0564	36.42
zzd	$p312$	$x-1, x-y+1, -z$	0.5017	0.2827	0.6907	0.0796	46.98
zze	$p321$	$x-y, 1-y, -z$	0.4273	0.0227	0.3979	0.0796	47.09
sql-c**	$pnam$	$1/2, 1/2+y, -z$	0.0	0.1213	0.2237	0.2051	73.39
cmi	$p\bar{4}$	$1-y, 1+x, -z$	0.2659	0.2557	0.3257	0.1654	75.31
cmi-c	$p\bar{4}$	$1+y, -1-x, -z$	0.2027	0.2162	0.6165	0.0544	70.53
cmi-c*	$p\bar{4}b2$	$1-y, 1+x, -z$	0.2442	0.2481	0.4286	0.1611	68.27
cmx	$p\bar{4}$	$1+y, -1-x, -z$	0.2515	0.2497	0.6175	0.0628	71.37
cmv	$p4/n$	$2-y, 1+x, -z$	−0.0219	0.6153	0.4564	0.1368	73.56
cmt	$p\bar{3}1m$	$1, 1-x, -z$	0.1340	0.0	0.2664	0.2282	95.05
cmt	$p\bar{3}$	$x-y, x, -z$	0.9524	0.7619	0.3086	0.2500	90.00
cmw	$p\bar{3}$	$x-y-1, x, -z$	0.6154	0.1538	0.5095	0.1111	90.00
cmz	$p\bar{3}$	$2-y, 2-x+y, -z$	0.2313	−0.2721	0.5832	0.0500	90.00

$\equiv 2\tan^{-1}(2^{1/4})$. Some weaves for small u, v are also illustrated in Fig. 2. The warp and weft are shown as black and white, respectively, so that the pattern of the design emerges. Weavings 1, v have interesting designs with intertwined spirals. We have not seen these described before. Fig. 3 shows the design for **sql-w120** ($u = 1$, $v = 20$).

3.2. Weavings with bundles of threads

Worsted fabrics are woven with a yarn of multiple threads. In the simplest such case there can be parallel threads. A plain weave with parallel threads is known as *basket weave* and it has a regular (transitivity 1 1 1) embedding, as do all the weaves of the previous section. Basket weave was earlier assigned the symbol **wvc** by Liu *et al.* (2018) who, however, gave the transitivity as 1 2 1. We note here a better embedding with transitivity 1 1 1. We give this the symbol **sql-w-c** to emphasize that the basket weave can be considered as two interwoven plain weaves (Fig. 4). (The appended symbol **-c** is RCSR notation for an interpenetrating pair of structures.) If the **sql-w-c** structure were to be drawn for the optimal embedding of cylindrical threads, the figure shows that the lattice plane is not fully occupied; thus the structure is more suitable as a weaving of laths (as in basket making). However, when the weaving is made with (approximately) cylindrical threads, as used in shirt-making, then it is known as 'Oxford weave'.

Regular weavings of pairs are also possible for the other regular biaxial weaves. These are given the symbol **sql-w12-c**, **sql-w23-c** *etc.* These structures are also depicted in Fig. 4 and data for optimum-girth embeddings are given in Table 2.

We identify three further regular structures in this section. In these, the single thread of plain weave is replaced by a helical pair of entwined threads in the spirit of worsted fabrics (known as *stuffs*). We use the extension **-ww** to signify worsted weave and our structures are **sql-ww, sql-ww*** and **sql-ww**.** These patterns are illustrated in Fig. 5, and optimum-girth data are in Table 2. In **sql-w**, warp and weft helices of the same handedness are woven as in the plain weave. **sql-w*** is similar, but now the helices are alternately of opposite hand-

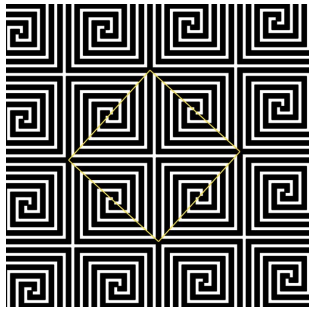

Figure 3
The design (weaving pattern) of **sql-w120**. Note the interleaved spirals.

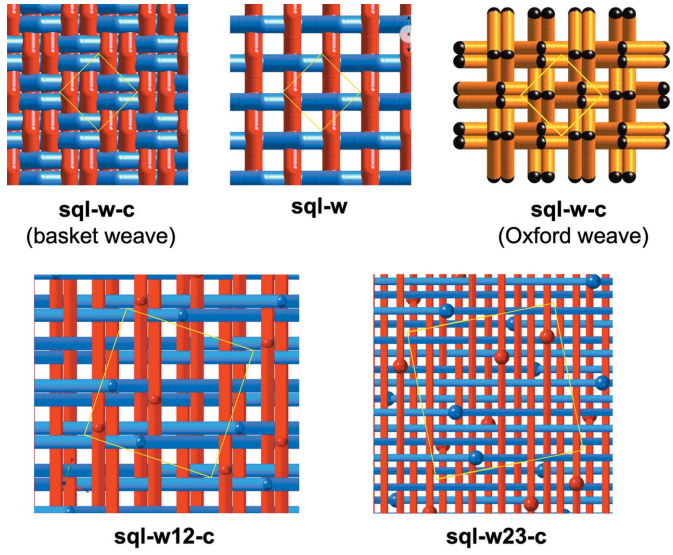

Figure 4
Weaves using pairs of threads. Top: left, **sql-w-c** drawn with 'flat' threads to be area filling; centre, with one half of the threads missing, illustrating that **sql-w-c** is two interwoven **sql-w** weaves; right, **swl-w-c** drawn with cylindrical threads of maximum girth. Bottom: two more double-thread weaves, illustrating their open nature.

edness and the structure is achiral. In **sql-w**** the warp and weft helices interpenetrate – see the detail in Fig. 5.

4. Triaxial weaves

We have only a small group of regular triaxial weaves. They all have symmetry *p*622 and are portrayed in Fig. 6 with crystallographic data in Tables 1 and 2. The first is the kagome weave, **kgm**, commonly used in basket making – especially with bamboo laths – and also known as bamboo weave. It is an open weave. With 'planar' (*i.e.* lath-like) threads, only one quarter of the area of the lattice plane is occupied. Indeed, the name comes from the Japanese for 'basket eye'. Kagome weave has the property of Borromean rings that, if one component is removed, the other two fall apart. Notice in the figure that green threads are over red, red over blue, and blue over green so every colour is, in a sense, layered 'in the middle' of the other two.

A regular worsted version of kagome (**kgm-ww**), with helical pairs of threads in each direction, is also shown in Fig. 6.

Another regular triaxial weave has long been known as 'mad weave'. It is found commonly in bamboo weaves, particularly of platters. In contrast to kagome weave, if mad weave is made of 'planar' threads, the plane is fully covered. The resulting pattern is also presented in the figure.

Two other triaxial structures are illustrated in Fig. 7. These can be considered as weavings derived from the 3-coordinated (3-c) **hcb** net. To make weavings from 4-c (4-coordinated) nets, such as **sql** and **kgm**, each vertex is split into two. To make a weaving from a 3-c net, such as **hcb**, each vertex must be split into three. The resulting vertices must also be non-coplanar. This can be accomplished with symmetry *p*321, as shown in Fig. 7 for **hcb-w**. In this structure, zigzag threads run in three directions and their axes intersect to form a planar kagome net, so this structure is indeed a triaxial fabric weave. Note, however, that the angle at each corner is now quite small (∼47°) at optimum girth.

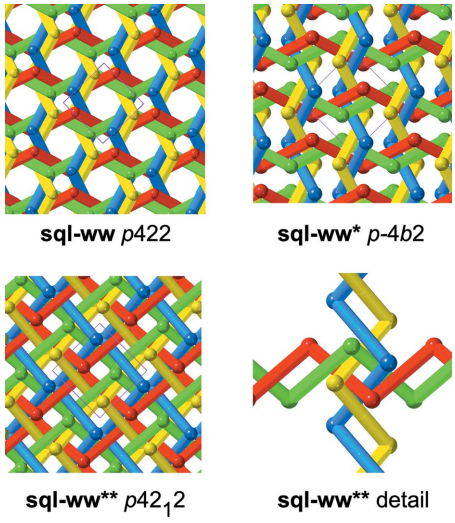

Figure 5
Regular weavings with helical bundles of threads ('worsted') in a simple weave pattern. Top left: all helices of the same handedness. Top right: weaving with helices of both handedness. Bottom left: a variation in which helices (but not individual threads) intersect, as shown in the detail in the bottom right.

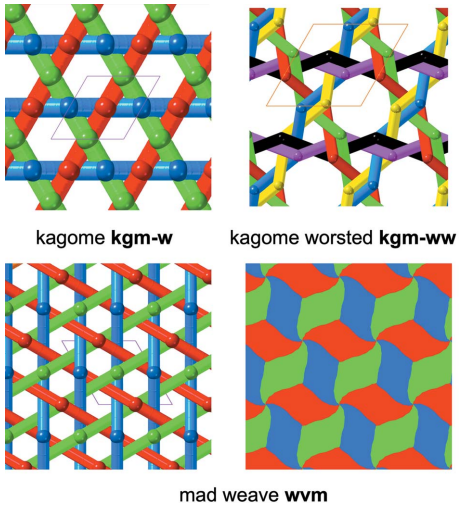

Figure 6
Regular triaxial weaves. Bottom right is the pattern when 'mad' weave is made with thin area-filling laths. All structures are chiral (symmetry *p*622).

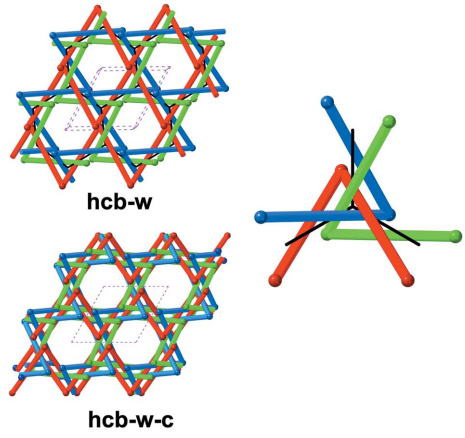

Figure 7
Top: **hcb-w**, a triaxial weave based on the **hcb** net (thin black lines). A detail of the triple crossing in **hcb-w** is shown on the right. Bottom: two such weaves interpenetrating, **hcb-w-c**.

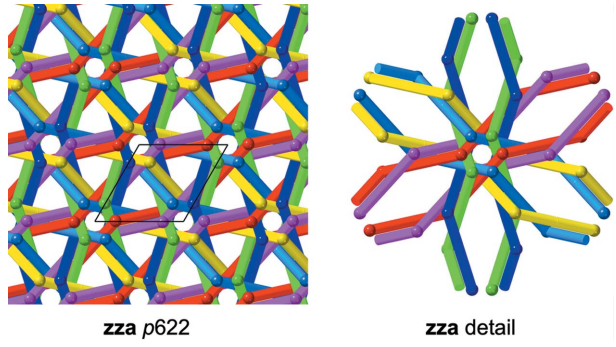

Figure 8
A regular triaxial weave, **zza**, with six pairs of helices crossing at vertices of a hexagonal lattice net (**hxl**).

Two such weaves can interpenetrate to form **hcb-w-c** with symmetry *p*622, as seen in the figure. Isolated in the figure is a detail of the 'triple crossing' around one parent **hcb** vertex.

We adduce another triaxial weave of bundles of threads with symmetry *p*622 and symbol **zza** (Fig. 8). In this lovely structure 12 threads converge on a crossing, as detailed in the figure. The crossing points are now the vertices of the hexagonal lattice net (**hxl**). This pattern is not possible with straight threads replacing the helical pairs because all thread axes are coplanar.

5. Some weavings of zigzag threads

In conventional fabric weaving the projection of the thread on the lattice plane is a straight line. In worsteds they are almost straight. By contrast, in weavings such as chain link and knitting, the projection of the thread is far from linear. Liu *et al.* (2018) show some such patterns but none had transitivity 1 1 1. Here (Fig. 9) we present some examples of regular weavings of zigzag threads. In optimum-girth embeddings the angle between rods is less than 60° as already noted above for **hcb-w**. It is likely that there are many more examples with even smaller angles but, although beautifully intricate, they are less likely to be feasible targets for designed synthesis and have not been systematically explored.

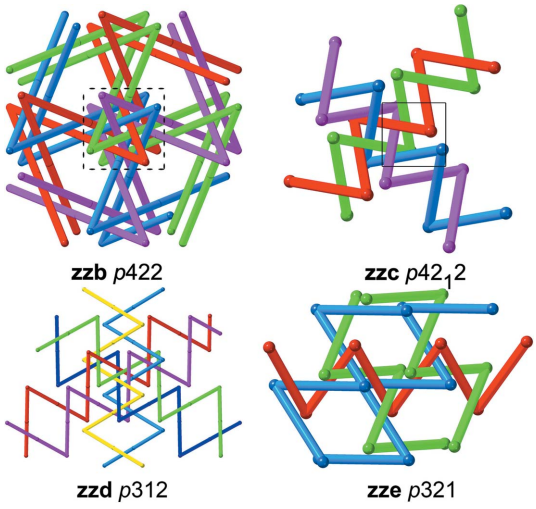

Figure 9
Four regular patterns of chiral weavings of zigzags with angles less than 60°.

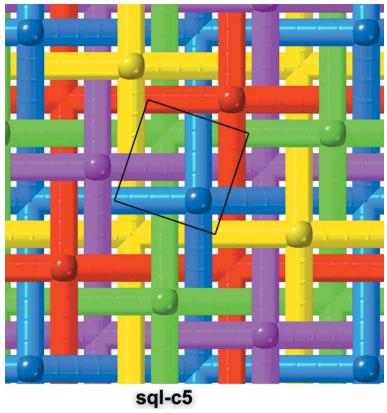

Figure 10
sql-c5, a pattern formed from the regular interweaving of five **sql** nets.

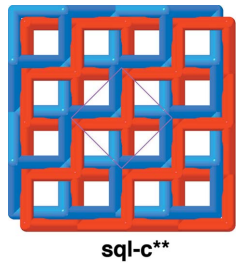

Figure 11
sql-c**, a regular rectangular interweaving of two **sql** nets.

6. Interwoven 2-periodic nets

6.1. Interwoven square lattice nets (sql)

There is an infinite family of regular 2-periodic weavings of **sql** nets. This is simply related to the family of regular biaxial thread weaves described in Section 3.1. Thus, with symmetry *p*4/*n* (origin choice 2), those threads had a vertex at 3/4, 1/4, *z*. If instead we place a vertex at 1/4, 1/4, *z*, the same link produces interpenetrating **sql** nets. The number of nets, *t*, is given by the same *u*, *v* knight's-move vector components as before, by $t = u^2 + v^2$. Specifically, $t = 5, 13, 17, \ldots$ as explained in that earlier section. Fig. 10 illustrates **sql-c5**. The pattern is such that the weaving of any two overlapping rings is over, over, under, under ... repeated periodically, and a ring of one net is linked to two each of the other four nets so the *catenation number* is 8. More generally for **sql-c*n*** the catenation number is $2(n - 1)$.

We note here also a regular rectangular interweaving of two **sql** nets, symbol **sql-c**** (Fig. 11). This has symmetry *pman* and catenation number 2. A vertex- and edge-transitive tetragon does not have to have equal angles: it could be diamond shaped. To obtain equal angles we set $a = b$. Data for maximum girth with this constraint are given in Table 2.

6.2. Regular weavings of honeycomb (hcb) nets

A 2-periodic pattern, **hxl-w** (Fig. 12, left), of three interwoven **hcb** nets has symmetry $p\bar{3}1m$. Just as plain weave **sql-w** is derived by splitting the square lattice net into two components, and the kagome weave **kgm-w** is derived by splitting the kagome net into three, the **hxl-w** pattern is generated by splitting each vertex of the 6-coordinated hexagonal lattice net (**hxl**) into two 3-coordinated vertices.

This pattern is well known in ornamentation and is also found frequently in crystal structures (Alexandrov *et al.*, 2017, and references therein). Like the kagome weave, it has the Borromean property that although the nets are interwoven, removal of one component leaves the other two unlinked. It can be seen from the figure that blue is over green, green over

red, and red over blue. In what follows we refer to such a combination as a 'Borromean triplet'. Note that the catenation number of each hexagon is zero.

Two **hxl-w** (= **hcb-c3**) weaves of lower-symmetry ($p312$) embedding can be combined to form **hcb-c6** with symmetry $p622$ as illustrated in Fig. 13. The two **-c3** are Borromean triplets but, as also shown in the figure, nets of one triplet are directly catenated with the nets of the other. Specifically, each ring is catenated with four rings of each of the three others for a catenation number of 12.

Delgado-Friedrichs & O'Keeffe (2009) also gave the rules for allowed generalized knight's moves $u\mathbf{a} + v\mathbf{b}$ on an infinite *hexagonal* chess board. They are: (*a*) u, v co-prime; (*b*) $uv \neq 3n$ (n an integer); (*c*) $v > 2u$. A (hexagonal) supercell of edge $u\mathbf{a} + v\mathbf{b}$ will contain $t = u^2 - uv + v^2$ points. t is a prime number of the form $6n + 1$ (n an integer) or a product of such primes (*e.g.* 7×7, 7×13, ...).

If now, with symmetry $p\bar{3}$, a vertex at $0, 0, z$ is joined to one at $u, v, -z$, a pattern of $3t$ interpenetrating **hcb** nets is obtained. The factor of '3' arises from the fact that an edge of **hcb** is $1/\sqrt{3}$ times a unit-cell edge. The simplest possibility is **hcb-c21** ($u, v, t = 1, 3, 7$) illustrated in Fig. 12 (right). Note that in these structures there is just one vertex per unit cell.

A related family **hcb-c*t*** is obtained as follows. Again with symmetry $p\bar{3}$, a point at $1/3, 2/3, z$ is joined to

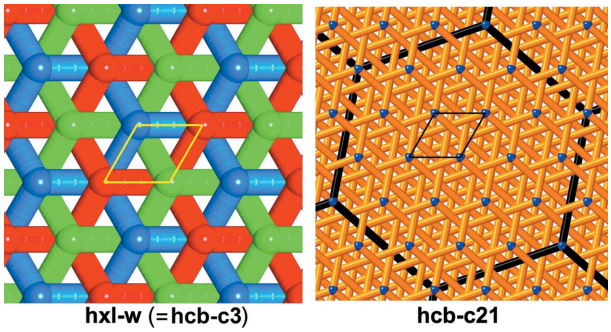

Figure 12
Two regular weavings of honeycomb (**hcb**) nets with just one vertex per unit cell. Left: **hxl-w**, with three interwoven **hcb** nets; right: **hcb-c21**, with 21 interwoven **hcb** nets.

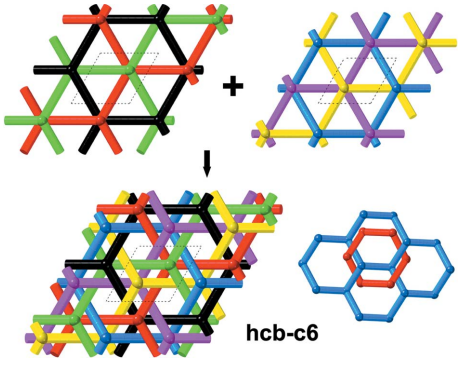

Figure 13
Two **hxl-w** (= **hcb-c3**) weaves (top) combining to form **hcb-c6** (below). On the right is shown how one ring (red) of one **hxl-w** is catenated to four rings of one triplet of the other triplet.

$$u + v = 3n + 1 : \ 1/3 + (v - 2u)/3, 2/3 + (2v - u)/3, -z$$

$$u + v = 3n + 2 : \ 1/3 + (2v - u)/3, 2/3 + (v - 2u)/3, -z.$$

Now there are two vertices per unit cell. The simplest possibility is **hcb-c7** ($u, v, t = 1, 3, 7$), shown in Fig. 14.

The pattern of weaving in **hcb-c7** is particularly interesting. As for **hcb-c3**, no two nets are interwoven but there are Borromean triplets. Each one of the seven nets is 'in the middle', in the sense that it is under three nets and over three. It may be seen from the figure that each of these sets of three is a Borromean triplet and there are accordingly 14 distinct triplets – one 'above' and one 'below' each of the seven nets. To describe the pattern of the weaving, a tiling with seven vertices (represented by seven colours), 21 edges (each colour is a neighbour to the other six) and 14 triangular faces (for the Borromean triplets) is required. This has genus 0 and should be inscribed on a torus, but can be shown as a 2-periodic tiling with coloured vertices, as in Fig. 15. The colouring in the figure is the same as in Fig. 14, and each differently coloured triangle in Fig. 15 corresponds to a Borromean triplet in Fig. 14. Also,

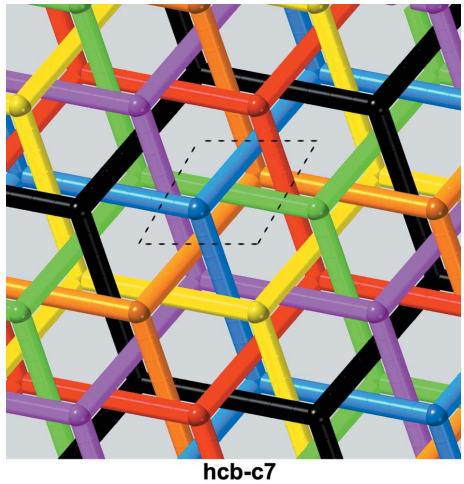

Figure 14
The pattern of weaving of seven **hcb** nets (each of a different colour) in **hcb-c7**. Note that each colour always crosses above three other colours and always crosses below the three remaining colours.

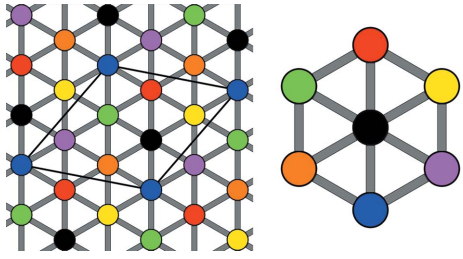

Figure 15
The pattern of weaving in **hcb-c7**. Each vertex corresponds to a similarly coloured layer in Fig. 14. The 14 triangles with distinct vertex colourings correspond to the 14 Borromean triplets in **hcb-c7**. On the right, the six colours surrounding black show the six Borromean triplets involving the black layer. The two triplets of second-neighbour vertices correspond to the Borromean triplets (green–yellow–blue and red–magenta–orange) 'above' and 'below' a black **hcb** net.

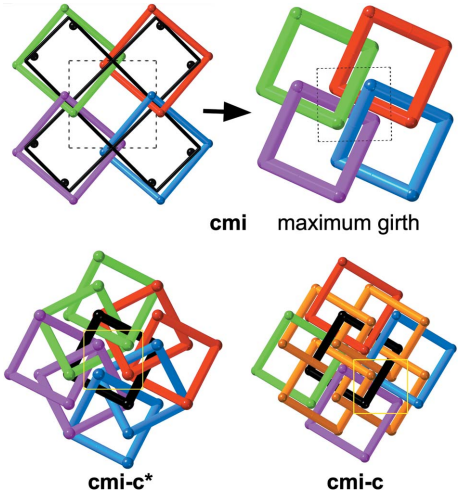

Figure 16
Top: derivation of the simplest tetragonal chain mail, **cmi**, from the square lattice net (**sql**). Bottom: two modes of interweaving of **cmi**. In **cmi-c** (bottom right) the two sets are not directly linked.

as indicated in Fig. 15, it can be seen which Borromean triplets are 'above' and 'below' a given layer. They are the two triplet second-neighbour colours, which are shown on the surrounding hexagon. Thus, for black, these are green–yellow–blue and red–magenta–orange.

7. Polycatenanes ('chain mail')

Linked loops are commonly called 'polycatenanes' in chemistry. 2-Periodic patterns are also called 'chain mails' after the medieval armour (*maille* is a French word for 'stitch'). Liu *et al.* (2018) described a number of these. Here we identify two families of regular patterns.

7.1. Tetragonal chain mail

Just as biaxial thread weave can be generated by splitting the vertices of a square lattice (**sql**) into components, a related splitting can generate linked tetragons. In the simplest case there will be four corners per unit cell, with two above and two below the lattice plane, and for square symmetry the only possibility is $p\bar{4}$. Fig. 16 illustrates the generation of the simple regular tetragonal chain mail, **cmi**. Each tetragon is linked to four others (catenation number 4). At optimum girth (data in Table 2) the angle is about 75°.

We show also **cmi-c** and **cmi-c***, which are pairs of interpenetrating **cmi** patterns. These are generated by adding a glide component to the symmetry. Specifically, *b*-glide symmetry augments the layer group to $p\bar{4}b2$, to generate **cmi-c***, and *n*-glide symmetry in the lattice plane augments the layer group symmetry to $p4/n$, for **cmi-c**. In **cmi-c*** both components are directly connected by Hopf links and the catenation number is now 8. In **cmi-c** the rings of one component are not linked to those of the other.

There are infinitely more patterns of linked tetragons. As there are just four points related by a $\bar{4}$ axis in the unit cell, the possibilities can be systematically enumerated as follows. In the case of **cmi-c** an edge is defined as the link from x, y, z to $1 + y, -1 - x, -z$ (space group $P\bar{4}$, second-origin choice). Systematic variation of x, y and zc/a, for fixed a, in the 3-periodic group $P\bar{4}$, was carried out to determine maximum girth, as described in Section 2. Additionally, for a given x, y a maximum girth can be found by varying just zc/a, and a contour (or intensity) map of that girth as a function of x and y prepared. As we see in Fig. 17, the map has regions of finite girth (coloured) bounded by lines of zero girth (black), where edges intersect. Structures in a given region are isotopic but edges must be broken and reformed to pass from one region to the other, so generally structures in separate regions are not isotopic. In some instances, they are symmetry-related variants.

We identified over a hundred regions in the tetragonal chain-mail (TCM) system. Maximum-girth data for the 12 largest-maximum-girth structures are given in Table 3. Note that the isotopic structures TCM2 and TCM3 (indicated in Fig. 17) correspond to separate 'attractor' maximum-girth peaks within a single region (*i.e.* are not separated by a zero-girth boundary). Illustrations of these structures are attached as supporting information. They include examples of catenation number for every multiple of 4 from 4 to 24. For each $p\bar{4}$ structure there are also corresponding $p\bar{4}b2$ and $p4/n$ structures.

We present in Fig. 18 the next two simplest, after **cmi**, tetragonal chain mails (TCM2 and TCM5) with catenation

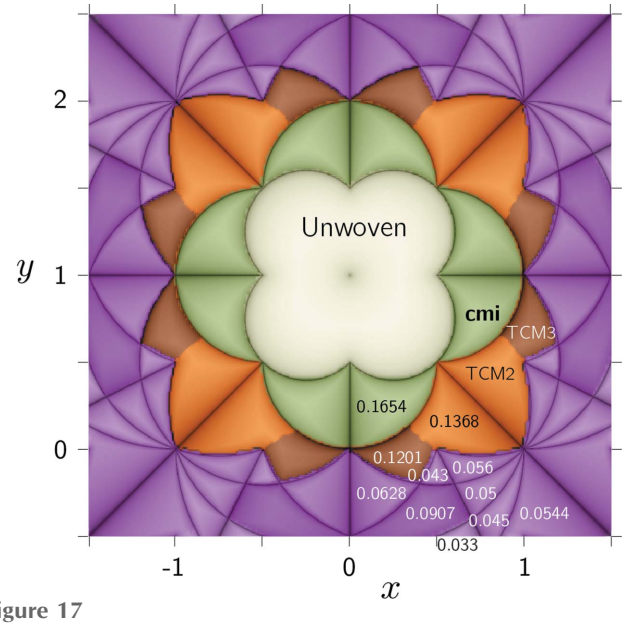

Figure 17
Structure map for the tetragonal chain-mail system, **cmi**. x and y are the in-plane crystallographic coordinates of the 'from' vertex. The intensity of the image is proportional to the maximum girth of sticks, found by adjusting zc/a at each x, y. Different colours represent regions within which structures are attracted to a local maximum-girth value. The dark lines represent places where the maximum girth is zero, where sticks are forced to intersect by symmetry. At these boundaries, sticks must pass through each other to enter an adjoining region. The values of some of the peak girths are indicated. Some regions contain two maximum-girth attractors for the same weave, such as TCM2 and TCM3 (see illustration in supporting information.)

Table 3
Data for 12 regions in the tetragonal chain-mail (TCM) system.

The maximum-girth structure is given the RCSR code **cmi**. All weaves are based on sticks connecting from (x, y, z) to $(1 - y, 1 - x, -z)$ in space group $p\bar{4}$. The structure map is shown in Fig. 17.

Symbol	x	y	zc/a	Girth	Angle (°)
cmi	0.2659	0.2557	0.3257	0.1654	75.31
TCM2	0.5218	0.1152	0.4557	0.1368	73.59
TCM3	0.3794	−0.0146	0.3976	0.1201	77.74
TCM4	0.4500	−0.3500	0.7115	0.0907	70.53
TCM5	0.2515	−0.2497	0.6175	0.0628	71.37
TCM6	0.6794	−0.1018	0.4622	0.0563	78.28
TCM7	1.0135	−0.4189	0.8719	0.0544	70.53
TCM8	0.7675	−0.2392	0.4973	0.0500	79.12
TCM9	0.8543	−0.3744	0.5329	0.0450	79.73
TCM10	0.4879	−0.1490	0.5241	0.0434	74.89
TCM11	0.9404	−0.5074	0.5653	0.0410	80.30
TCM12	0.6400	−0.5088	0.6753	0.0331	75.31

numbers 8 and 12, respectively. These both have symmetry $p\bar{4}$ and, again, catenated pairs are generated by changing the symmetry to $p\bar{4}b2$ and $p4/n$. In **cmi**, rings are linked in pairs but, as clarified in Fig. 18, in TCM2 rings are linked in fours, forming a torus link (4, 4). In TCM5, we see in the figure that each tetragon is linked to five others.

As discussed by Liu *et al.* (2018), it appears not possible to have *regular* chain mail with *planar* rings. The most regular is a rectangular pattern (European four-in-one, symbol **cmk**) with transitivity 1 2 1.

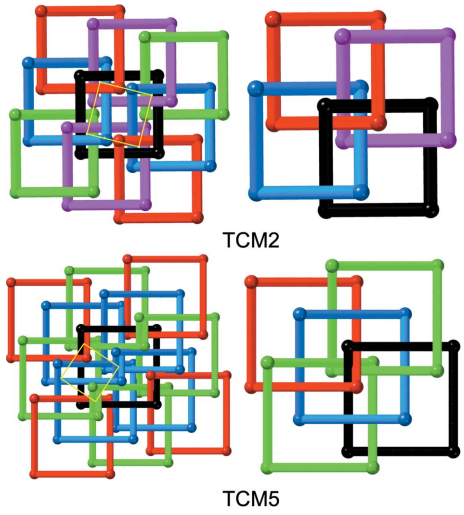

Figure 18
Two patterns of tetragonal chain mail, with catenation numbers 8 (top) and 12 (bottom). In each case the detail on the right shows the pattern whereby simple loops connect into complicated links.

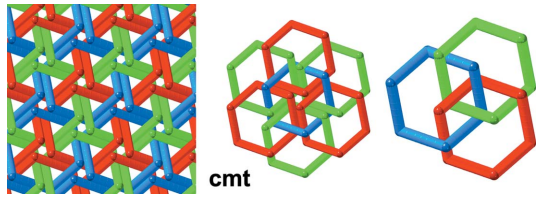

Figure 19
Regular hexagonal chain mail **cmt**. In the centre is the pattern of overlap with one ring (blue). If the blue ring is removed, the others are not linked. On the right is a Borromean triplet of rings. Note how red is always above green; green is always above blue; and blue is always above red.

7.2. Hexagonal chain mail

Of the patterns described by Liu *et al.* (2018) we find just one, symbol **cmt**, that has a regular embedding. It is also the one example of 2-periodic chain mail forming the basis of a crystal structure (Thorp-Greenwood *et al.*, 2015).[1] This structure has an embedding with symmetry $p\bar{3}1m$, but has a larger-girth embedding with lower symmetry $p\bar{3}$, shown in Fig. 19. We give data for both chain-mail symmetries in Table 2. **cmt** can be generated by inscribing hexagons in the hexagonal faces of **hxl-w** (= **hcb-c3**). In a wide-ranging investigation we generated a structure map (Fig. 20), similar to that for tetragonal chain mail, now using $p\bar{3}$ and links from x, y, z to $x - y, x, -z$. Data for ten large-girth structures are listed in Table 4, which includes two structures that lie outside the range of the illustrated map. Notable is the fact that the optimized girth is always $1/n$, n an integer, and the optimum angle at each corner is always 90°. **cmt** has girth 1/4.

As shown in Fig. 21 the structure comprises hexagons inscribed in the faces of **hxl-w** (= **hxg-c3**). The rings are not directly catenated but form Borromean triplets. The structure with the next-largest girth is HCM2 with girth = 1/9. This is again derived from **hxl-w** by inscribing hexagons in **hxl-w** but

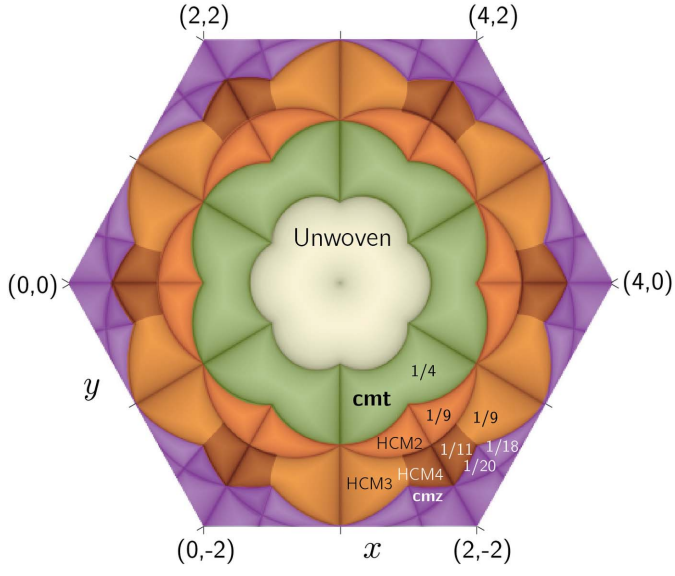

Figure 20
Structure map for the hexagonal chain-mail system, **cmt**. The peaks in girth within each region are the reciprocals of integers, $1/n$. The values of some of the peak girths are indicated.

[1] These authors, correctly in our opinion, refer to their structure as Borromean chain mail. However, one finds on the web at http://katlas.org/wiki/L10n107 and https://commons.wikimedia.org/wiki/File:Borromean-chainmail-tile.svg a quite different structure. This has four components, so is not strictly 'Borromean', even though no two components are linked. A piecewise linear representation is shown in the supporting information.

Table 4
Data for ten regions in the hexagonal chain-mail (HCM) system.

The maximum-girth structure is given the RCSR code **cmt**. All weaves are based on sticks connecting from (x, y, z) to $(x - y, x, -z)$ in space group $p\bar{3}$. The structure map is shown in Fig. 20.

Symbol	x	y	zc/a	Girth	Angle (°)
cmt	1.2381	0.1905	0.3086	0.2500	90.00
HCM2	0.8947	0.1579	0.4215	0.1111	90.00
HCM3	0.8462	0.4615	0.5095	0.1111	90.00
HCM4	0.6491	0.1930	0.5151	0.0909	90.00
HCM5	0.2807	0.2456	0.6556	0.0714	90.00
HCM6	0.4762	0.7619	0.7127	0.0625	90.00
HCM7	0.6154	0.4615	0.5884	0.0556	90.00
HCM8	0.5034	0.2721	0.5832	0.0500	90.00
HCM9	0.4615	0.5128	0.6537	0.0500	90.00
HCM10	0.1183	1.0753	0.9165	0.0400	90.00

now the hexagons form additional Borromean triplets as shown in the figure.

The structures next in girth are again 1/9 (HCM3) and 1/11 (HCM4). These two are in fact isotopic as they correspond to two attractor maximum-girth peaks in the same region of the structure map. This structure is now derived from **hcb-c7** as **cmt** is derived from **hcb-c3**, as shown in Fig. 22. There is again a related structure (HCM10, girth = 1/20) in which the inscribed hexagons form additional Borromean triplets, as shown in the figure.

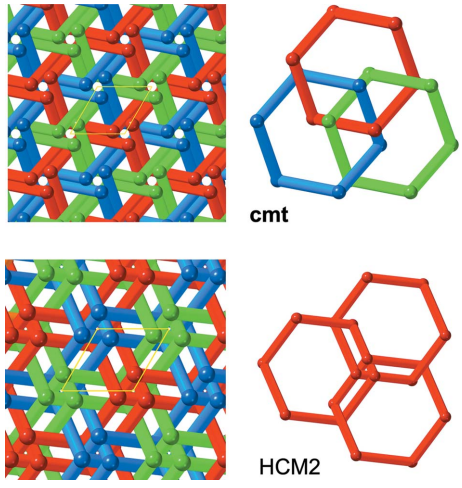

Figure 21
Top: the structure of **cmt**, with girth = 1/4. Bottom: the next member in the hexagonal chain-mail family, HCM2, which has girth = 1/9.

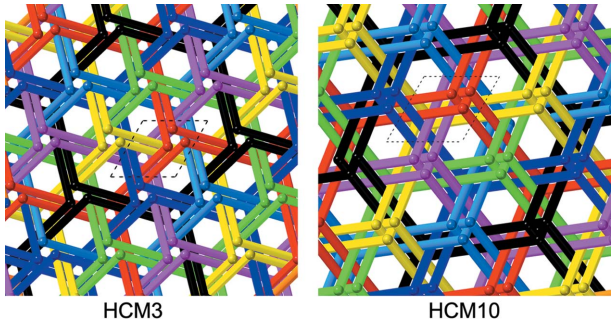

Figure 22
Two regular chain-mail patterns derived from **hcb-7**. Note the extra Borromean triplets in HCM10 (*cf.* Fig. 21).

Next, in order of girth, are: HCM5, with girth = 1/12, which is formed from **hcb-c13**; and HCM6, girth = 1/13, formed from **hcb-c19**. These are illustrated in the supporting information.

At the intersections of the zero-girth lines in the structure map, vertices and edges overlap. If we remove the degeneracy by allowing overlapping corners and sticks to merge, new higher-coordination, non-zero-girth weaves appear. Maximum girth = $1/n$, as before, but with different sets of integer-n values.

8. Summary and conclusions

In this work we have limited ourselves to structures that, in a piecewise linear representation, have just one kind of vertex (corner) and one kind of link (stick). In the structures made from infinite threads they are necessarily simple zigzags with axes that intersect to form a simple planar 2-periodic net. Such materials are termed *fabric* weavings (Liu *et al.*, 2018). We have not considered *chain-link* weavings for which, in the 2-periodic case, the axes of the threads form parallel lines. This class of weaving includes knitting. The symmetry must be rectangular or lower and, we believe, there are no *regular* chain-link weavings. We note, however, that knitted materials are expected to have significantly different mechanical properties from woven fabrics (*e.g.* Poincloux *et al.*, 2018); consequently a crystallographic description and classification of such structures would be useful.

We recall that a motivation for our work is to develop a library of structures that could form the basis of designed syntheses of targeted crystalline materials. In this context it is important to remember that, while knitting uses just one thread, and biaxial or triaxial weaving just two or three, the tactic of the chemical approach to woven crystal structures is to link (polymerize) pre-assembled components into woven threads (Wadhwa *et al.*, 2016; Zhao *et al.*, 2017; Liu *et al.*, 2016). Although many of the patterns reported here are unlikely to appear in fabrics, they may well appear in crystal structures.

Finally, we draw attention to an interesting recent paper by Nishiyama (2019) which shows that fluid flow may well adopt weaving patterns.

References

Alexandrov, E. V., Blatov, V. A. & Proserpio, D. M. (2017). *CrystEngComm*, **19**, 1993–2006.
Delgado-Friedrichs, O. & O'Keeffe, M. (2003). *Acta Cryst.* A**59**, 351–360.
Delgado-Friedrichs, O. & O'Keeffe, M. (2009). *Acta Cryst.* A**65**, 360–363.
Evans, M. E., Robins, V. & Hyde, S. T. (2015). *Proc. R. Soc. A*, **471**, 20150254.
Flapan, E. (1988). *Discrete Appl. Math.* **19**, 157–166.
Grosicki, C. J. (1977). *Watson's Advanced Textile Design.* London: Newnes–Butterworths.
Grünbaum, B. & Shephard, G. C. (1980). *Math. Mag.* **53**, 139–161.

Grünbaum, B. & Shephard, G. C. (1985). *Ann. New York Acad. Sci.* **440**, 279–298.
Grünbaum, B. & Shephard, G. C. (1986). *Discrete Geom.* **60**, 155–192.
Grünbaum, B. & Shephard, G. C. (1988). *Am. Math. Mon.* **95**, 5–30.
Li, M., Li, D., O'Keeffe, M. & Yaghi, O. M. (2014). *Chem. Rev.* **114**, 1343–1370.
Liu, Y., Ma, Y., Zhao, Y., Sun, X., Gándara, F., Furukawa, H., Liu, Z., Zhu, H., Zhu, C., Suenaga, K., Oleynikov, P., Alshammari, A. S., Zhang, X., Terasaki, O. & Yaghi, O. M. (2016). *Science*, **351**, 365–369.
Liu, Y., O'Keeffe, M., Treacy, M. M. J. & Yaghi, O. M. (2018). *Chem. Soc. Rev.* **47**, 4642–4664.
Nelder, J. A. & Mead, R. (1965). *Comput. J.* **7**, 308–313.
Nishiyama, T. (2019). *Acta Cryst.* A**75**, 798–813.
O'Keeffe, M., Peskov, M. A., Ramsden, S. J. & Yaghi, O. M. (2008). *Acc. Chem. Res.* **41**, 1782–1789.
Poincloux, S., Adda-Bedia, M. & Lechenault, F. (2018). *Phys. Rev. X*, **8**, 021075.
Press, W. H., Teukolsky, S. A., Vetterling, W. T. & Flannery, B. P. (1992). *Numerical Recipes in C: The Art of Scientific Computing.* Cambridge, New York: Cambridge University Press.
Roth, R. L. (1993). *Geom. Dedicata*, **48**, 191–210.
Stasiak, A., Katritch, V. & Kauffman, L. H. (1998). *Ideal Knots*, Vol. 19. Singapore: World Scientific.
Thompson, B. & Hyde, S. T. (2018). *Isr. J. Chem.* **58**, 1144–1156.
Thorp-Greenwood, F. L., Kulak, A. N. & Hardie, M. J. (2015). *Nat. Chem.* **7**, 526–531.
Treacy, M. M. J., Randall, K. H., Rao, S., Perry, J. A. & Chadi, D. J. (1997). *Z. Kristallogr.* **212**, 768–791.
Wadhwa, N. R., Hughes, N. C., Hachem, J. A. & Mezei, G. (2016). *RSC Adv.* **6**, 11430–11440.
Yaghi, O. M., O'Keeffe, M., Ockwig, N. W., Chae, H. K., Eddaoudi, M. & Kim, J. (2003). *Nature*, **423**, 705–714.
Zhao, Y., Guo, L., Gándara, F., Ma, Y., Liu, Z., Zhu, C., Lyu, H., Trickett, C. A., Kapustin, E. A., Terasaki, O. & Yaghi, O. M. (2017). *J. Am. Chem. Soc.* **139**, 13166–13172.